The Astrophysical Journal, 628:923–930, 2005 August 1

ON THE METHOD OF ESTIMATING EMISSION ALTITUDE FROM RELATIVISTIC PHASE SHIFT IN PULSARS

R. T. Gangadhara
Indian Institute of Astrophysics, Koramangala, II Block, Bangalore 560034, India; ganga@iiap.res.in
Received 2004 March 31; accepted 2005 April 14

ABSTRACT

The radiation by relativistic plasma particles is beamed in the direction of field-line tangents in the corotating frame, but in an inertial frame it is aberrated toward the direction of rotation. We have revised the relation of aberration phase shift by taking into account the magnetic colatitude and azimuth of the emission spot and the plasma rotation velocity. In the limit of the small-angle approximation, the aberration phase shift becomes independent of the inclination angle α and the sight line impact angle β. However, at larger altitudes or larger rotation phases, the shift does depend on α and β. We have given an expression for the phase shift in the intensity profile by taking into account aberration, retardation, and polar cap currents.

Subject headings: pulsars: general — radiation mechanisms: nonthermal — stars: magnetic fields — stars: neutron

1. INTRODUCTION

The profile morphology and polarization of pulsars have been widely attempted to be interpreted in terms of emission in dipolar magnetic field lines (e.g., Radhakrishnan & Cooke 1969; Sturrock 1971; Ruderman & Sutherland 1975; Lyne & Manchester 1988; Blaskiewicz et al. 1991; Rankin 1983a, 1983b, 1990, 1993; Hibschman & Arons 2001). Most of the radio emission models assume that (1) radiation is emitted by the relativistic secondary pair plasma, (2) beamed radio waves are emitted in the direction of field-line tangents, and (3) emitted radiation is polarized in the plane of dipolar field lines or in the perpendicular directions.

From the theoretical point of view, it is highly preferable to know the precise altitude of the radio emission region in the pulsar magnetosphere. By knowing the emission altitude, one can infer the probable plasma density, rotation velocity, magnetic field strength, field-line curvature radii, etc., that prevail in the radio emission region. For estimating the radio emission altitudes, two kinds of methods have been proposed: (1) the purely geometric method, which assumes that the pulse edge is emitted from the last open field lines (e.g., Cordes 1978; Gil & Kijak 1993; Kijak & Gil 2003), and (2) the relativistic phase shift method, which assumes that the asymmetry in the conal components phase location, relative to the core, is due to the aberration-retardation phase shift (e.g., Gangadhara & Gupta 2001, hereafter GG01). By estimating the phase lag of the polarization angle inflection point with respect to the centroid of the intensity pulse, Blaskiewicz et al. (1991) have estimated the emission heights. The results of the purely geometric method are found to be in rough agreement with those of Blaskiewicz et al. (1991). However, compared to the geometric method, the emission heights estimated from relativistic phase shift are found to be notably larger, particularly in the case of nearly aligned rotators (Gupta & Gangadhara 2003, hereafter GG03). Dyks et al. (2004, hereafter DRH04), by revising the relation for aberration phase shift given by GG01, have reestimated the emission heights. In the small-angle approximation, they have found that the revision furnishes a method for estimating radio emission altitudes that is free of polarization measurements and does not depend on α, the magnetic axis inclination angle, and β, the sight line impact angle. By assuming that the beamed radio waves are emitted in the direction of field-line tangents, Gangadhara (2004, hereafter G04) has solved the viewing geometry in an inclined and rotating dipole magnetic field.

In § 2 we derive the angle between the corotation velocity of particles/plasma bunches and the dipolar magnetic field. Using the magnetic colatitude and azimuth of the emission spot in an inclined and rotating dipole, we have derived the phase shift due to aberration, retardation, and polar cap current in § 3 and the emission radius in § 4. In § 5 we compare the shifts due to different processes.

2. ANGLE BETWEEN PLASMA ROTATION VELOCITY AND DIPOLAR MAGNETIC FIELD

Consider an inclined and rotating magnetic dipole $\hat{\boldsymbol{m}}_t$ with rotation axis $\hat{\boldsymbol{\Omega}}$, as shown in Figure 1. The angles α and ϕ' are the magnetic axis inclination angle and the rotation phase, respectively. Assume that the relativistic secondary plasma flows along the dipolar field lines and emits the beamed radiation in the direction of field-line tangents ($\hat{\boldsymbol{b}}_{0t}$). In a nonrotating case, to receive such an emission the sight line $\hat{\boldsymbol{n}}$ must line up with $\hat{\boldsymbol{b}}_{0t}$. Let Q be the emission point on a field line at which $\hat{\boldsymbol{n}} = (\sin\zeta,\ 0,\ \cos\zeta)$ is parallel to $\hat{\boldsymbol{b}}_{0t}$, where $\zeta = \alpha + \beta$ and β is the sight line impact angle relative to $\hat{\boldsymbol{m}}_t$. The angles $\angle\mathrm{QOR} = \theta$ and $\angle\mathrm{QRT} = \phi$ are the magnetic colatitude and azimuth of Q relative to $\hat{\boldsymbol{m}}_t$, respectively, while $\angle\mathrm{QOZ} = \theta'$ and $\angle\mathrm{XOS} = \phi'$ are the colatitude and azimuth of Q relative to the rotation axis, respectively.

If $\boldsymbol{r}$ is the position vector of Q, then the angle between $\boldsymbol{r}$ and $\hat{\boldsymbol{\Omega}}$ is given by

$$\cos\theta' = \hat{\boldsymbol{\Omega}}\cdot\hat{\boldsymbol{r}} = \cos\alpha\cos\theta - \sin\alpha\sin\theta\cos\phi, \qquad (1)$$

where the unit vector $\hat{\boldsymbol{r}} = \boldsymbol{r}/|\boldsymbol{r}|$ and the expressions for θ and ϕ as functions of ϕ', α, and β are given in G04.

For the field line that lies in the meridional plane, defined by $\hat{\boldsymbol{\Omega}}$ and $\hat{\boldsymbol{m}}_t$, we have $\theta'_{\min} = \alpha + \theta_{\min}$. The magnetic colatitude $\theta_{\min}$ of Q can be obtained by setting $\phi' = 0$ in equation (9) of G04:

$$\theta_{\min} = \frac{1}{2}\arccos\left[\frac{\cos(2\beta) + \sqrt{2}\cos\beta\sqrt{17 + \cos(2\beta)} - 1}{6}\right]$$
$$\approx \frac{2}{3}\beta + O(\beta)^3 \quad \text{for } \beta \ll 1. \qquad (2)$$

This is the minimum value that θ takes at $\phi' = 0$.

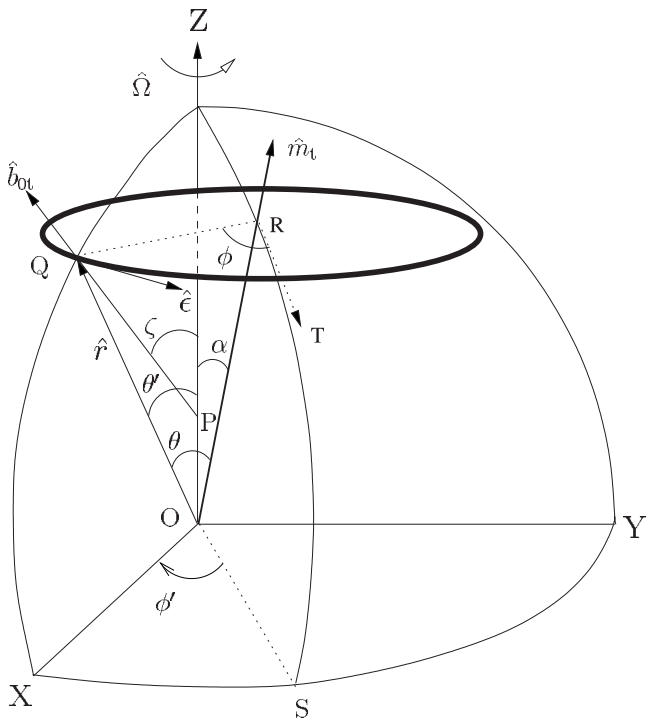

FIG. 1.—Viewing geometry of emission beam. The heavy ellipse represents the cone of emission centered on the magnetic axis $\hat{\boldsymbol{m}}_t$. The arcs ZQX, ZRS, ZY, and XSY represent the great circles centered at O (star center). The magnetic colatitude ϕ and the phase angle ϕ' of the emission spot are measured from the meridional ($\hat{\boldsymbol{\Omega}}$, $\hat{\boldsymbol{m}}_t$)-plane. They have signs such that ϕ' is positive while ϕ is negative on the trailing side, and vice versa on the leading side.

The rotation velocity of the plasma particle (bunch) at Q is given by

$$\boldsymbol{v}_{\rm rot} = \boldsymbol{\Omega}\times\boldsymbol{r} = \Omega r \sin\theta' \hat{\boldsymbol{\epsilon}}, \tag{3}$$

where $\boldsymbol{\Omega}$ is the pulsar angular velocity and the unit vector $\hat{\boldsymbol{\epsilon}}$ represents the direction of rotation. Consider a Cartesian coordinate system XYZ, with the Z-axis parallel to the rotation axis and the X-axis lying in the fiducial plane defined by $\hat{\boldsymbol{n}}$ and $\hat{\boldsymbol{\Omega}}$. Let Θ be the angle between the field-line tangent $\hat{\boldsymbol{b}}_{0t}$ and $\hat{\boldsymbol{\epsilon}}$, then we have

$$\hat{\boldsymbol{\epsilon}} = \cos\Theta\hat{\boldsymbol{\epsilon}}_{\parallel} + \sin\Theta\hat{\boldsymbol{\epsilon}}_{\perp}, \tag{4}$$

where the unit vectors $\hat{\boldsymbol{\epsilon}}_{\parallel}$ and $\hat{\boldsymbol{\epsilon}}_{\perp}$ are parallel and perpendicular to $\hat{\boldsymbol{b}}_{0t}$, respectively. Therefore, the angle Θ is given by

$$\cos\Theta = \hat{\boldsymbol{\epsilon}}\cdot\hat{\boldsymbol{b}}_{0t} = \frac{a_1}{\sqrt{(1+4a_2^2)a_3}}, \tag{5}$$

where

$$a_1 = \sin\alpha\sin\phi, \quad a_2 = \cot\theta,$$

$$a_3 = \frac{\cos^2\alpha\cos^2\phi + a_2^2\sin^2\alpha + a_2\cos\phi\sin(2\alpha) + \sin^2\phi}{1+a_2^2}.$$

We have plotted Θ as a function of rotation phase ϕ' for different α in Figure 2. It shows $\Theta = 90^\circ$ for the field lines that lie in the meridional plane ($\phi' = 0$), but for other field lines it is $<90^\circ$ on the leading side and $>90^\circ$ on the trailing side.

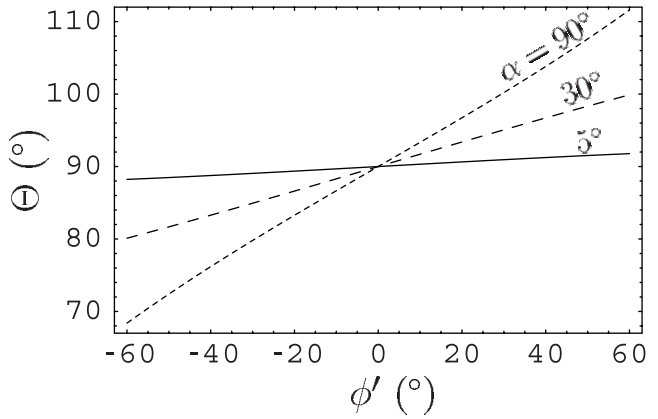

FIG. 2.—Angle Θ vs. rotation phase ϕ' for different values of α and a fixed $\beta = 2^\circ$.

But for an aligned rotator ($\alpha = 0^\circ$), it is 90° for all the field lines.

3. PHASE SHIFT OF RADIATION EMITTED BY A PARTICLE (BUNCH)

Since the pulsar spin rate is quite high, the rotation effects such as aberration and retardation play an important role in the morphology of pulse profiles. For an observer in an inertial frame, the radiation beam gets phase shifted due to the corotation of plasma particles and the difference in emission radii.

Since the radiation by a relativistic particle is beamed in the direction of the velocity, to receive it the sight line must align with the particle velocity within the angle $1/\gamma$, where γ is the Lorentz factor. The particle velocity is given by

$$\boldsymbol{v} = \kappa c\hat{\boldsymbol{b}}_{0t} + \boldsymbol{v}_{\rm rot}, \tag{6}$$

where c is the speed of light. By substituting for $\boldsymbol{v}_{\rm rot}$ from equation (3) into equation (6), we obtain

$$\boldsymbol{v} = (\kappa c + \Omega r\sin\theta'\cos\Theta)\hat{\boldsymbol{b}}_{0t} + \Omega r\sin\theta'\sin\Theta\hat{\boldsymbol{\epsilon}}_{\perp}. \tag{7}$$

By assuming $|\boldsymbol{v}| \sim c$, from equation (7) we obtain the parameter

$$\kappa = \sqrt{1 - \left(\frac{\Omega r}{c}\right)^2 \sin^2\theta'\sin^2\Theta} - \frac{\Omega r}{c}\sin\theta'\cos\Theta. \tag{8}$$

In Figure 3, we have plotted κ as a function of r for different α. It shows $\kappa \sim 1$ for $r/r_{\rm LC} \ll 1$, but at large r it decreases

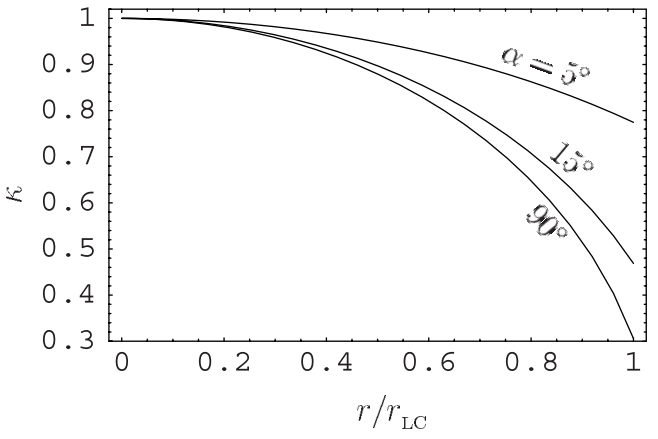

FIG. 3.—Parameter κ vs. $r/r_{\rm LC}$ for different α at $\phi' = 0^\circ$ and $\beta = 2^\circ$.

from unity due to increase in rotation velocity, where $r_{\rm LC}$ is the light cylinder radius. Machabeli & Rogava (1994), by considering the motion of a bead inside a rotating linear tube, have deduced a similar behavior in the velocity components of the bead.

Using equation (3), we can solve equation (4) for $\hat{\boldsymbol{\epsilon}}_\perp$ and obtain

$$\hat{\boldsymbol{\epsilon}}_\perp = \frac{\hat{\boldsymbol{\Omega}}\times\hat{\boldsymbol{r}}}{\sin\theta'\sin\Theta} - \cot\Theta\hat{\boldsymbol{b}}_{0t}. \tag{9}$$

Let ψ be the angle between the rotation axis and $\boldsymbol{v}$, then we have

$$\begin{aligned}\cos\psi &= \hat{\boldsymbol{\Omega}}\cdot\hat{\boldsymbol{v}} \\ &= \cos\zeta\left[\sqrt{1-\left(\frac{\Omega r}{c}\right)^2\sin^2\theta'\sin^2\Theta} - \frac{\Omega r}{c}\sin\theta'\cos\Theta\right] \\ &= \kappa\cos\zeta,\end{aligned} \tag{10}$$

where $\hat{\boldsymbol{v}} = \boldsymbol{v}/|\boldsymbol{v}|$. For $r/r_{\rm LC} \ll 1$, this reduces to $\psi \sim \zeta$.

3.1. *Aberration Angle*

If η is the aberration angle, then we have

$$\cos\eta = \hat{\boldsymbol{b}}_{0t}\cdot\hat{\boldsymbol{v}} = \frac{\kappa c + \Omega r\sin\theta'\cos\Theta}{|\boldsymbol{v}|}, \tag{11}$$

$$\sin\eta = \hat{\boldsymbol{\epsilon}}_\perp\cdot\hat{\boldsymbol{v}} = \frac{\Omega r}{|\boldsymbol{v}|}\sin\theta'\sin\Theta. \tag{12}$$

Therefore, from equations (11) and (12), we obtain

$$\tan\eta = \frac{\Omega r}{c}\frac{\sin\theta'\sin\Theta}{\sqrt{1-(\Omega r/c)^2\sin^2\theta'\sin^2\Theta}}. \tag{13}$$

Hence, the radiation beam, which is centered on the direction of $\boldsymbol{v}$, gets tilted (aberrated) with respect to $\hat{\boldsymbol{b}}_{0t}$ due to rotation.

For $\Omega r/c \ll 1$, this can be approximated as

$$\tan\eta \approx \frac{\Omega r}{c}\sin\theta'\sin\Theta. \tag{14}$$

3.2. *Aberration Phase Shift*

Consider Figure 4 in which ZAD, ZBX, ZCY, and DXY are the great circles centered on the neutron star. The small circle ABC is parallel to the equatorial great circle DXY. The unit vector $\hat{\boldsymbol{b}}_{0t}$ represents a field-line tangent, which makes the angle ζ with respect to the rotation axis ZO. The velocity unit vector $\hat{\boldsymbol{v}}$ is inclined by the angles η and ψ with respect to $\hat{\boldsymbol{b}}_{0t}$ and ZO, respectively. We resolve the vectors $\hat{\boldsymbol{b}}_{0t}$ and $\hat{\boldsymbol{v}}$ into the components parallel and perpendicular to the rotation axis:

$$\hat{\boldsymbol{b}}_{0t} = \sin\zeta\hat{\boldsymbol{b}}_{0t\perp} + \cos\zeta\hat{\boldsymbol{\Omega}}, \tag{15}$$

$$\hat{\boldsymbol{v}} = \sin\psi\hat{\boldsymbol{v}}_\perp + \cos\psi\hat{\boldsymbol{\Omega}}, \tag{16}$$

where the unit vectors $\hat{\boldsymbol{b}}_{0t\perp}$ and $\hat{\boldsymbol{v}}_\perp$ lie in the plane of the small circle ABC. Next, by solving for $\hat{\boldsymbol{b}}_{0t\perp}$ and $\hat{\boldsymbol{v}}_\perp$, we obtain

$$\hat{\boldsymbol{b}}_{0t\perp} = \frac{1}{\sin\zeta}\left(\hat{\boldsymbol{b}}_{0t} - \cos\zeta\hat{\boldsymbol{\Omega}}\right), \tag{17}$$

$$\hat{\boldsymbol{v}}_\perp = \frac{1}{\sin\psi}\left(\hat{\boldsymbol{v}} - \cos\psi\hat{\boldsymbol{\Omega}}\right). \tag{18}$$

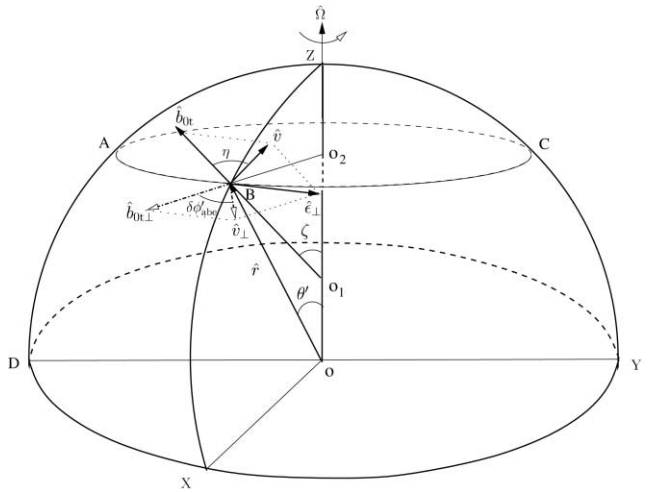

FIG. 4.—Celestial sphere describing the aberration phase shift of pulsar radio emission, where η is the aberration angle and $\delta\phi'_{\rm abe}$ is the corresponding phase shift.

By taking the scalar product with $\hat{\boldsymbol{b}}_{0t\perp}$ on both sides of equation (18), we obtain

$$\cos\left(\delta\phi'_{\rm abe}\right) = \hat{\boldsymbol{v}}_\perp\cdot\hat{\boldsymbol{b}}_{0t\perp} = \frac{1}{\sin\psi}\left(\hat{\boldsymbol{v}}\cdot\hat{\boldsymbol{b}}_{0t\perp} - \cos\psi\hat{\boldsymbol{\Omega}}\cdot\hat{\boldsymbol{b}}_{0t\perp}\right). \tag{19}$$

Since $\hat{\boldsymbol{\Omega}}$ and $\hat{\boldsymbol{b}}_{0t\perp}$ are orthogonal, we have

$$\cos\left(\delta\phi'_{\rm abe}\right) = \frac{1}{\sin\psi}\left(\hat{\boldsymbol{v}}\cdot\hat{\boldsymbol{b}}_{0t\perp}\right). \tag{20}$$

Using $\hat{\boldsymbol{b}}_{0t\perp}$ from equation (17), we obtain

$$\cos\left(\delta\phi'_{\rm abe}\right) = \frac{1}{\sin\psi}\frac{\left(\hat{\boldsymbol{v}}\cdot\hat{\boldsymbol{b}}_{0t} - \cos\zeta\hat{\boldsymbol{v}}\cdot\hat{\boldsymbol{\Omega}}\right)}{\sin\zeta}. \tag{21}$$

By substituting for $\hat{\boldsymbol{v}}\cdot\hat{\boldsymbol{b}}_{0t}$ and $\hat{\boldsymbol{v}}\cdot\hat{\boldsymbol{\Omega}}$ from equations (11) and (10), we obtain

$$\cos\left(\delta\phi'_{\rm abe}\right) = \frac{1}{\sin\psi}\frac{(\cos\eta - \cos\zeta\cos\psi)}{\sin\zeta}. \tag{22}$$

Substituting for η again from equation (11), we obtain

$$\cos\left(\delta\phi'_{\rm abe}\right) = \frac{1}{\sin\zeta\sin\psi}\left(\kappa + \frac{\Omega r}{c}\sin\theta'\cos\Theta - \cos\zeta\cos\psi\right). \tag{23}$$

By substituting for κ from equation (10), we obtain

$$\cos\left(\delta\phi'_{\rm abe}\right) = \frac{1}{\sin\zeta\sin\psi}\left(\frac{\cos\psi}{\cos\zeta} + \frac{\Omega r}{c}\sin\theta'\cos\Theta - \cos\zeta\cos\psi\right). \tag{24}$$

This can be further reduced to

$$\cos\left(\delta\phi'_{\rm abe}\right) = \tan\zeta\cot\psi + \frac{\Omega r}{c}\frac{\sin\theta'\cos\Theta}{\sin\zeta\sin\psi}. \tag{25}$$

The aberration phase shift $\delta\phi'_{\rm abe}$ is plotted as a function of β in Figure 5 for different α in the two cases: (1) $\phi' = 0^\circ$ and

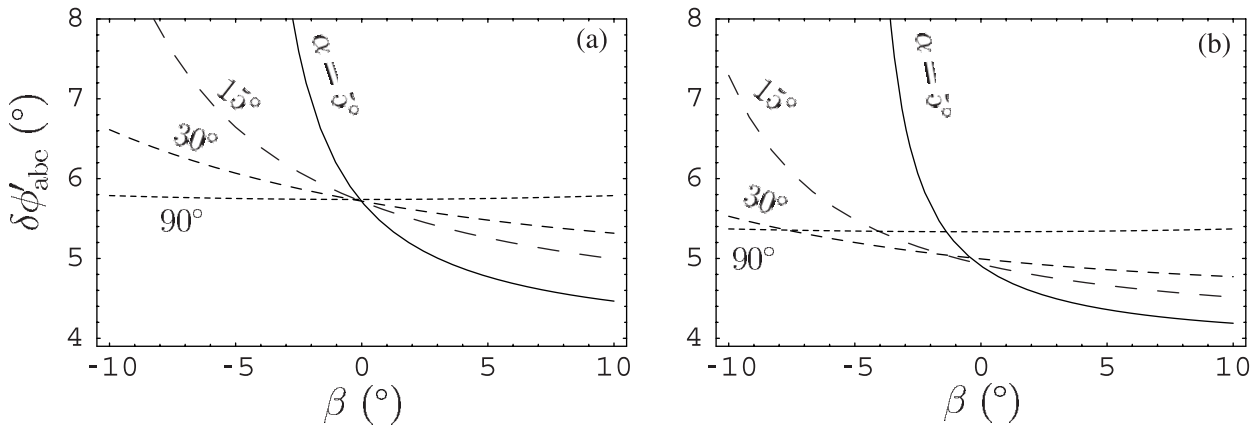

FIG. 5.—Aberration phase shift $\delta\phi'_{\rm abe}$ vs. sight line impact angle β for different α: (*a*) for $r_n = 0.1$ and $\phi' = 0^\circ$; (*b*) for $r_n = 0.1$ and $\phi' = 60^\circ$.

$r/r_{\rm LC} = 0.1$ and (2) $\phi' = 60^\circ$ and $r/r_{\rm LC} = 0.1$. Figure 5*a* shows for $\alpha \sim 90^\circ$, $\delta\phi'_{\rm abe} \approx r/r_{\rm LC}$, which is nearly independent of β. But for other values of α, it does depend on β: larger for $\beta < 0$ and smaller for $\beta > 0$. Since θ' decreases with $|\phi'|$ and $\Theta < 90^\circ$ on the leading side and >90° on the trailing side, $\delta\phi'_{\rm abe}$ is smaller in Figure 5*b* compared to its corresponding values in Figure 5*a*. Furthermore, we note that $\delta\phi'_{\rm abe}$ has a negative gradient with respect to $|\phi'|$ for both the signs of β. In Figure 6, $\delta\phi'_{\rm abe}$ is plotted as a function of ϕ' for different α and fixed $\beta = 4^\circ$. It is highest at large α and small $|\phi'|$.

For $r/r_{\rm LC} \ll 1$, we can series expand $\delta\phi'_{\rm abe}$ and obtain

$$\delta\phi'_{\rm abe} = b_1 r_n + b_2 r_n^2 + O(r_n)^3, \tag{26}$$

where $r_n = r/r_{\rm LC}$,

$$b_1 = \csc^2\zeta \sin\theta' \sqrt{-\cos(\Theta - \zeta)\cos(\Theta + \zeta)},$$
$$b_2 = -\cot^2\zeta \cos\Theta \sin\theta' b_1.$$

3.3. *Retardation Phase Shift*

Let θ_e, ϕ_e, and $\hat{\boldsymbol{r}}_e$ be the magnetic colatitude, azimuth, and position vector of the emission spot at the emission time, respectively. In the expressions for θ and ϕ (see eqs. [9] and [11] in G04) we replace ϕ' by $\phi' + \delta\phi'_{\rm abe}$ to obtain θ_e and ϕ_e. In Figure 7, using $r_n = 0.1$, $\alpha = 30^\circ$, and $\beta = 4^\circ$, we have plotted θ_e and ϕ_e as functions of ϕ'. It shows that both the minimum of

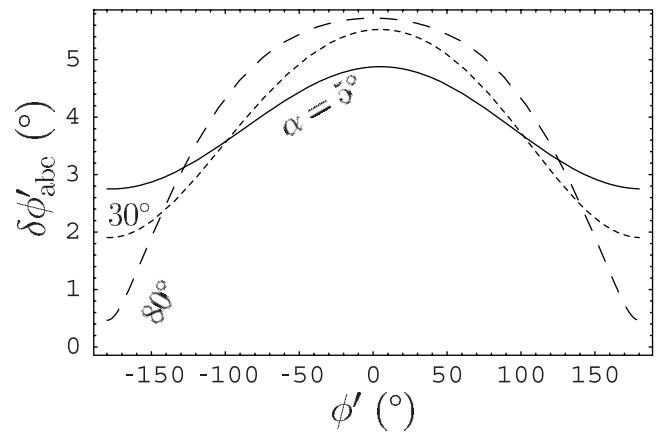

FIG. 6.—Aberration phase shift vs. phase ϕ'. Here $r_n = 0.1$, $\beta = 4^\circ$, and different α are as marked on the figure.

θ_e and zero-crossing point of ϕ_e are at the phase $\phi' = -5.5^\circ$. Using the values of θ_e and ϕ_e we find the unit vector $\hat{\boldsymbol{r}}_e$ (see eq. [2] in G04). For brevity, we drop the suffix on $\hat{\boldsymbol{r}}$. Note that $\phi' > 0$ on the trailing side (Fig. 1). Consider the emission radii r_1 and r_2 such that $r_1 < r_2$. The time taken by the signal emitted at the radius $\boldsymbol{r}_1$ is given by

$$t_1 = \frac{1}{c}(d - \boldsymbol{r}_1 \cdot \hat{\boldsymbol{n}}), \tag{27}$$

where d is the distance to the pulsar, and $\hat{\boldsymbol{n}} = (\sin\zeta,\ 0,\ \cos\zeta)$ is the unit vector pointing toward the observer. For another radius $\boldsymbol{r}_2$, the propagation time is given by

$$t_2 = \frac{1}{c}(d - \boldsymbol{r}_2 \cdot \hat{\boldsymbol{n}}). \tag{28}$$

The radiation emitted at the lower radius $\boldsymbol{r}_1$ takes more time to reach the observer than that emitted at $\boldsymbol{r}_2$. The time delay between the two signals is given by

$$\delta t = t_1 - t_2 = \frac{1}{c}(\boldsymbol{r}_2 \cdot \hat{\boldsymbol{n}} - \boldsymbol{r}_1 \cdot \hat{\boldsymbol{n}}). \tag{29}$$

By considering the neutron star center $\boldsymbol{r}_1 = 0$ as the reference and $\boldsymbol{r}_2 = \boldsymbol{r}$, we obtain

$$\delta t = \frac{r}{c}(\hat{\boldsymbol{r}} \cdot \hat{\boldsymbol{n}}). \tag{30}$$

Let σ be the angle between $\hat{\boldsymbol{r}}$ and $\hat{\boldsymbol{n}}$, then we have

$$\begin{aligned}\cos\sigma = \hat{\boldsymbol{r}} \cdot \hat{\boldsymbol{n}} = {} & \cos\zeta(\cos\alpha\cos\theta_e - \cos\phi_e \sin\alpha \sin\theta_e) \\ & - \sin\zeta\big[\sin\phi' \sin\phi_e \sin\theta_e \\ & - \cos\phi'(\cos\theta_e \sin\alpha + \cos\alpha\cos\phi_e \sin\theta_e)\big].\end{aligned} \tag{31}$$

The time delay δt of components emitted at lower heights shifts them to later phases of the profile by (e.g., Phillips 1992)

$$\delta\phi'_{\rm ret} = \Omega\,\delta t = \frac{\Omega r}{c}\cos\sigma. \tag{32}$$

In Figure 8, $\delta\phi'_{\rm ret}$ is plotted as a function of ϕ' for different α and fixed $\beta = 4^\circ$. At small α, it is nearly constant and larger. But at larger α, it falls with respect to $|\phi'|$, as $\hat{\boldsymbol{r}}$ inclines farther from $\hat{\boldsymbol{n}}$.

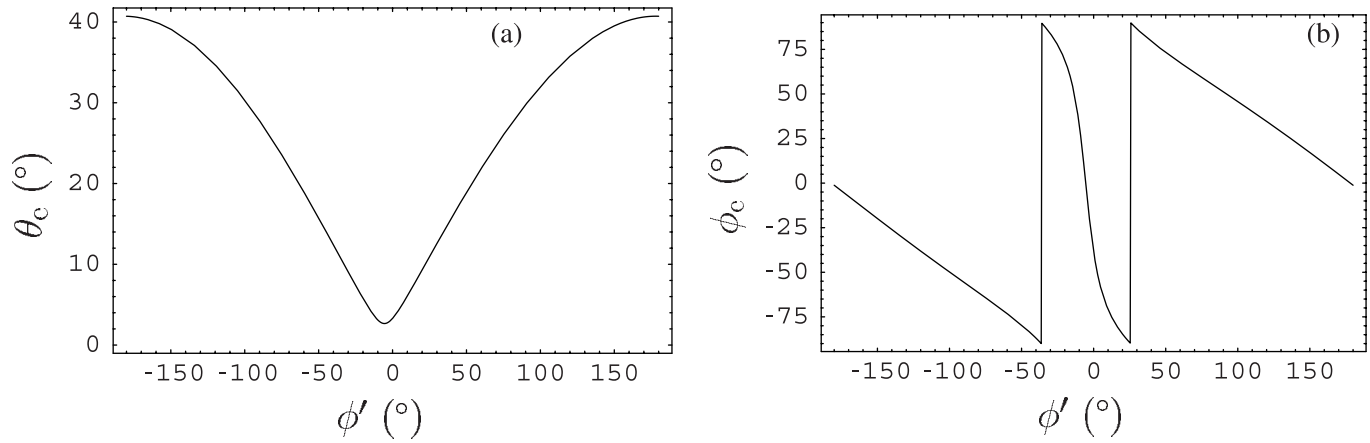

FIG. 7.—Magnetic colatitude θ_e and azimuth ϕ_e of emission spot vs. phase ϕ'. Here $r_n = 0.1$, $\alpha = 30^\circ$, and $\beta = 4^\circ$ for both panels.

For $r_n \ll 1$, we can find the series expansion

$$\delta\phi'_{\rm ret} = c_1 r_n + c_2 r_n^2 + O(r_n)^3, \tag{33}$$

where

$$c_1 = \cos(\Gamma - \theta),$$
$$c_2 = \frac{\sin\alpha \sin\zeta \sin\phi' \sin(\Gamma - \theta)(4\cot\theta + \tan\theta)}{3\sqrt{8 + \cos^2\Gamma}} b_1,$$

and Γ is the half-opening angle of the emission beam (see eq. [7] in G04).

3.4. *Relativistic Phase Shift*

Since the retardation and aberration phase shifts are additive, they can collectively introduce an asymmetry into the pulse profile (e.g., GG01). Therefore, the relativistic phase shift is given by

$$\delta\phi'_{\rm rps} = \delta\phi'_{\rm ret} + \delta\phi'_{\rm abe} = r_n \cos\sigma + \arccos\left(\tan\zeta \cot\psi + r_n \frac{\sin\theta' \cos\Theta}{\sin\zeta \sin\psi}\right). \tag{34}$$

In Figure 9, we have plotted $\delta\phi'_{\rm rps}$ as a function of ϕ' for different α in the two cases of $\beta = \pm 4^\circ$. It shows that $\delta\phi'_{\rm rps}$ reaches its maximum at $\phi' \sim 0$ and falls at large $|\phi'|$.

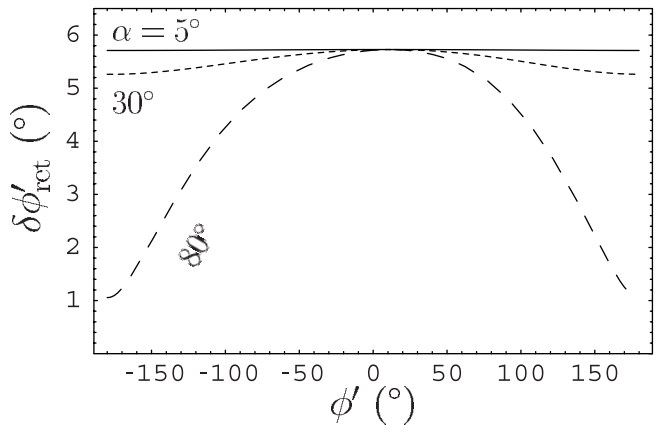

FIG. 8.—Retardation phase shift vs. phase ϕ'. Here $r_n = 0.1$, $\beta = 4^\circ$, and different α are as marked on the figure.

In the limit of $r_n \ll 1$, we can series expand $\delta\phi'_{\rm rps}$ and obtain

$$\delta\phi'_{\rm rps} = \mu_1 r_n + \mu_2 r_n^2 + O(r_n)^3, \tag{35}$$

where $\mu_1 = b_1 + c_1$ and $\mu_2 = b_2 + c_2$.

3.5. *Phase Shift Due to Polar Cap Current*

According to Goldreich & Julian (1969), the charged particles relativistically stream out along the magnetic field lines of a neutron star with aligned magnetic moment and rotation axis. Hibschman & Arons (2001) have shown that the field-aligned currents can produce a perturbation magnetic field $\boldsymbol{B}_1$ over the unperturbed dipole field $\boldsymbol{B}_0$ and can cause a shift in the polarization angle sweep. Here we intend to estimate the phase shift in the intensity profile due to the perturbation field $\boldsymbol{B}_1$. We assume that the observed radiation is emitted in the direction tangent to the field $\boldsymbol{B} = \boldsymbol{B}_0 + \boldsymbol{B}_1$. Using equations (D5) and (D6) given by Hibschman & Arons (2001), we find the Cartesian components of the perturbation field,

$$\boldsymbol{B}_1 = \left(2\frac{\mu}{r_{\rm LC}}\frac{\cos\alpha \sin\theta \sin\phi}{r^2},\ -2\frac{\mu}{r_{\rm LC}}\frac{\cos\alpha \sin\theta \cos\phi}{r^2},\ 0\right), \tag{36}$$

where μ is the magnetic moment. The Cartesian components of the unperturbed dipole are given by

$$\boldsymbol{B}_0 = \left[\frac{3}{2}\frac{\mu}{r^3}\sin(2\theta)\cos\phi,\ \frac{3}{2}\frac{\mu}{r^3}\sin(2\theta)\sin\phi,\ \frac{\mu}{r^3}\left(3\cos^2\theta - 1\right)\right]. \tag{37}$$

The magnetic field, which is tilted and rotated, is given by

$$\boldsymbol{B}_t = \Lambda \boldsymbol{B}, \tag{38}$$

where Λ is the transformation matrix given in G04.

The component of $\boldsymbol{B}_t$ perpendicular to the rotation axis is given by

$$\boldsymbol{B}_{t\perp} = \boldsymbol{B}_t - (\boldsymbol{B}_t \cdot \hat{\boldsymbol{\Omega}})\hat{\boldsymbol{\Omega}}. \tag{39}$$

Similarly, we find the perpendicular components of $\boldsymbol{B}_{0t} = \Lambda \boldsymbol{B}_0$,

$$\boldsymbol{B}_{0t\perp} = \boldsymbol{B}_{0t} - (\boldsymbol{B}_{0t} \cdot \hat{\boldsymbol{\Omega}})\hat{\boldsymbol{\Omega}}. \tag{40}$$

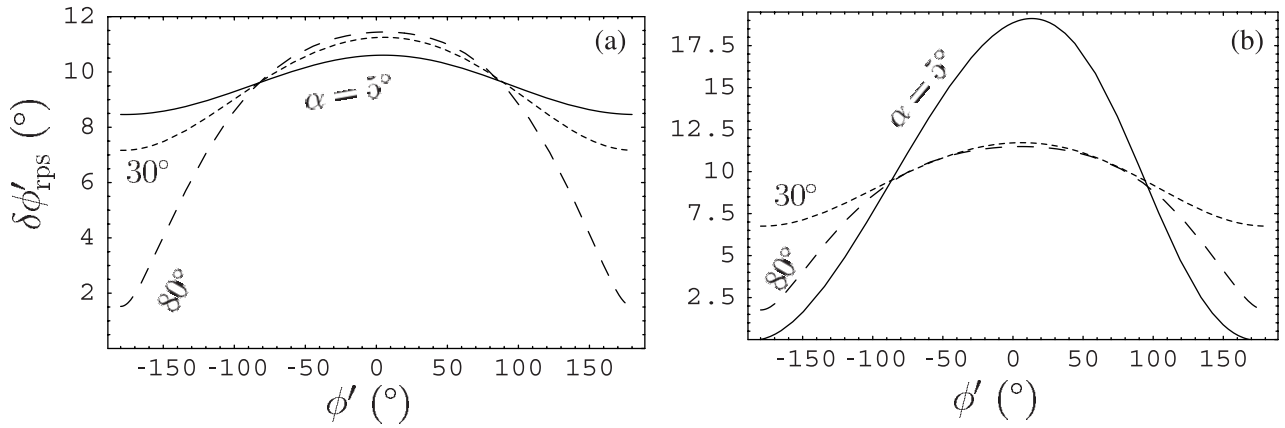

FIG. 9.—Relativistic phase shift vs. phase ϕ' for different α at $r_n = 0.1$: (*a*) $\beta = 4^\circ$ and (*b*) $\beta = -4^\circ$.

If $\delta\phi'_{\rm pc}$ is the phase shift in $\boldsymbol{B}_t$ due to the polar cap current, then we have

$$\cos\left(\delta\phi'_{\rm pc}\right) = \hat{\boldsymbol{b}}_{t\perp} \cdot \hat{\boldsymbol{b}}_{0t\perp} = \frac{B_{t\perp,x}}{|\boldsymbol{B}_{t\perp}|}, \tag{41}$$

where $\hat{\boldsymbol{b}}_{t\perp} = \boldsymbol{B}_{t\perp}/|\boldsymbol{B}_{t\perp}|$, the unit vector $\hat{\boldsymbol{b}}_{0t\perp} = \boldsymbol{B}_{0t\perp}/|\boldsymbol{B}_{0t\perp}|$ is parallel to the unit vector $\hat{\boldsymbol{x}}$ along the *X*-axis, and $B_{t\perp,x}$ is the *X*-component of $\boldsymbol{B}_{t\perp}$. If $\hat{\boldsymbol{y}}$ is the unit vector along the *Y*-axis, then we have

$$\sin\left(\delta\phi'_{\rm pc}\right) = \hat{\boldsymbol{b}}_{t\perp} \cdot \hat{\boldsymbol{y}} = \frac{B_{t\perp,y}}{|\boldsymbol{B}_{t\perp}|}. \tag{42}$$

Therefore, we have

$$\tan\left(\delta\phi'_{\rm pc}\right) = \frac{B_{t\perp,y}}{B_{t\perp,x}} = \frac{d_1 r_n}{d_2 + d_3 r_n}, \tag{43}$$

where

$$d_1 = \cos\phi' \sin(2\alpha) - 2\cos^2\alpha \tan\zeta,$$
$$d_2 = 3\cos\theta \tan\zeta,$$
$$d_3 = -\sin(2\alpha)\sin\phi'.$$

We have plotted $\delta\phi'_{\rm pc}$ as a function of ϕ' in Figure 10 by choosing $\alpha = 10^\circ$ and $r_n = 0.01$ and 0.1. It decreases with increasing $|\phi'|$ and is mostly negative, except in the case of $\beta < 0$, where it is positive over a small range of ϕ' near the $(\hat{\boldsymbol{\Omega}},\ \hat{\boldsymbol{m}}_t)$-plane. So, $\delta\phi'_{\rm pc}$ tries to reduce the relativistic phase shift $\delta\phi'_{\rm rps}$, except over a small range of ϕ' where it enhances the shift in the case of $\beta < 0$.

In the limit of $r_n \ll 1$, we can series expand equation (43) and obtain

$$\delta\phi'_{\rm pc} = \frac{d_1}{d_2} r_n - \frac{d_1 d_3}{d_2^2} r_n^2 + O(r_n)^3. \tag{44}$$

4. EMISSION RADIUS FROM PHASE SHIFT

We can find the net phase shift due to aberration, retardation, and polar cap current by adding equations (34) and (43):

$$\begin{aligned}\delta\phi' &= \delta\phi'_{\rm rps} + \delta\phi'_{\rm pc} \\ &= r_n \cos\sigma + \arccos\left(\tan\zeta \cot\psi + r_n \frac{\sin\theta' \cos\Theta}{\sin\zeta \sin\psi}\right) \\ &\quad + \arctan\left(\frac{d_1 r_n}{d_2 + d_3 r_n}\right).\end{aligned} \tag{45}$$

In Figure 11 we have plotted $\delta\phi'$ as a function of ϕ' in the four cases of r_n (0.01, 0.1, 0.2, and 0.3). It shows that $\delta\phi'$ reaches maximum near the $(\hat{\boldsymbol{\Omega}},\ \hat{\boldsymbol{m}}_t)$-plane and falls with respect to $|\phi'|$. Note that the magnitude of the gradient of $\delta\phi'$ with respect to $|\phi'|$ is higher than that of $\delta\phi'_{\rm rps}$. In the case of $\beta < 0$, we find that

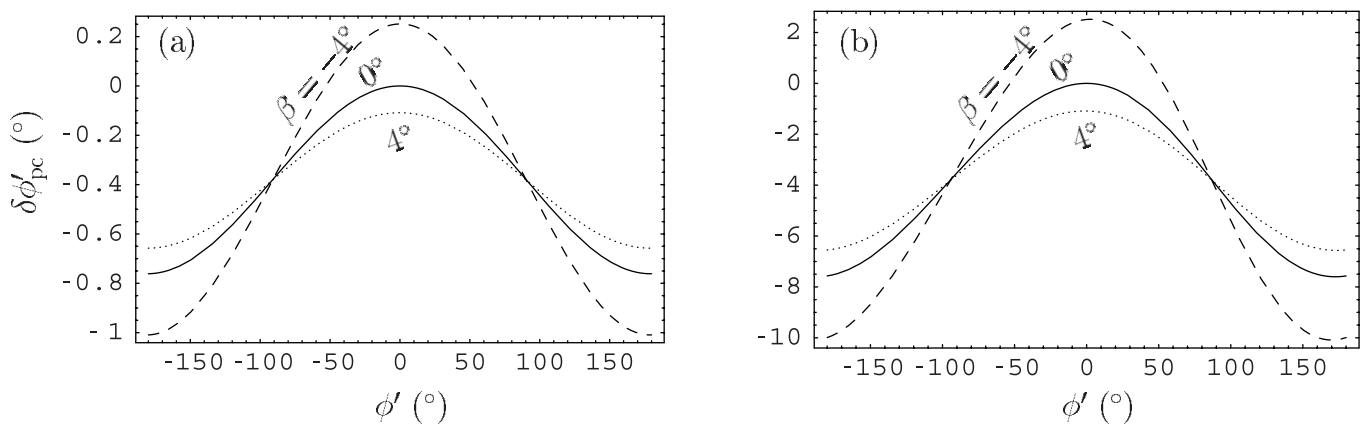

FIG. 10.—Phase shift $\delta\phi'_{\rm pc}$ due to polar cap current vs. phase ϕ' for $\alpha = 10^\circ$ at (*a*) $r_n = 0.01$ and (*b*) $r_n = 0.1$.

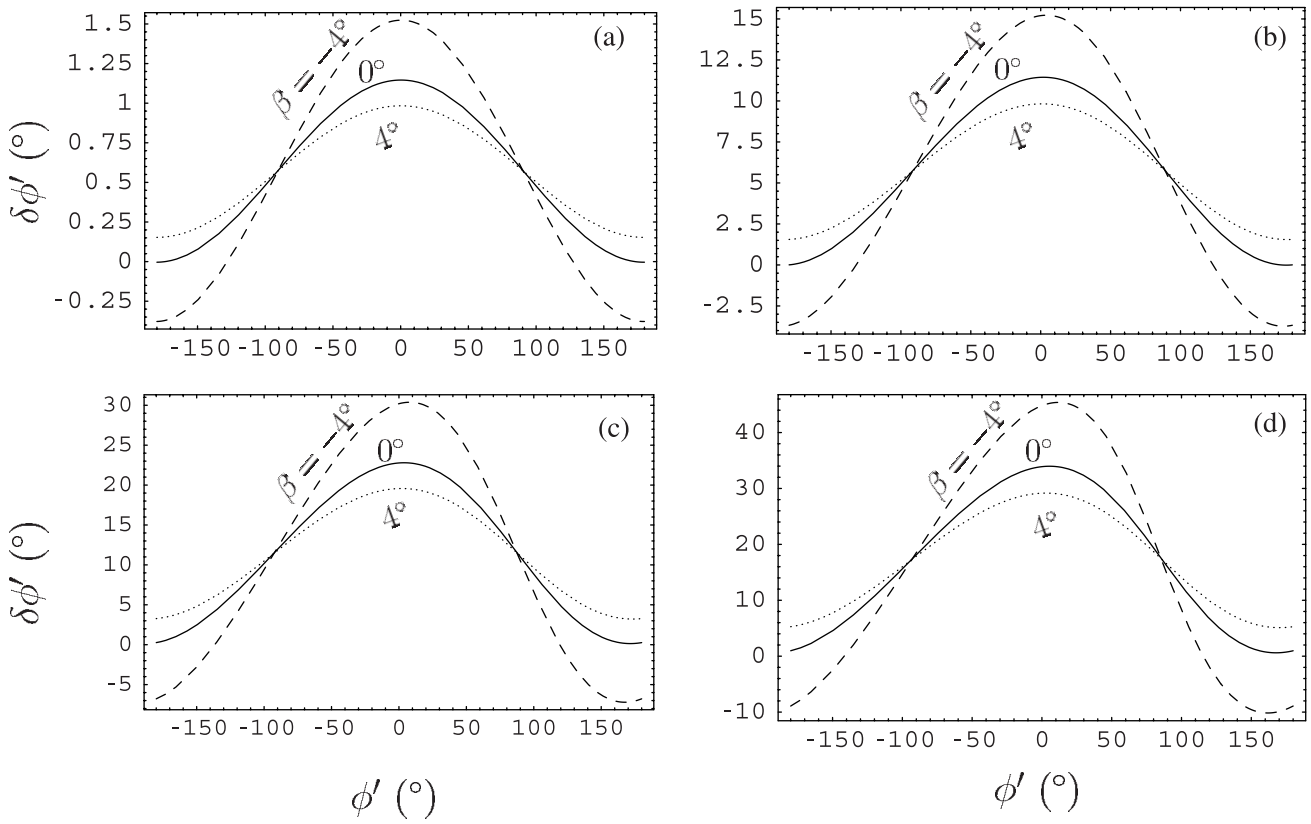

FIG. 11.—Net phase shift due to aberration, retardation, and polar cap current $\delta\phi'$ vs. phase ϕ'. Here $\alpha = 10^\circ$ and $r_n = 0.01$, 0.1, 0.2, and 0.3 for (*a*), (*b*), (*c*), and (*d*), respectively.

$\delta\phi'$ becomes negative at large $|\phi'|$ as the magnitude of $\delta\phi'_{\rm pc}$ exceeds the magnitude of $\delta\phi'_{\rm rps}$. At higher r_n, we note that $\delta\phi'$ is slightly asymmetric about $\phi' = 0$.

For $r_n \ll 1$, we obtain

$$\delta\phi' = \nu_1 r_n + \nu_2 r_n^2 + O(r_n)^3, \tag{46}$$

where $\nu_1 = \mu_1 + (d_1/d_2)$ and $\nu_2 = \mu_2 - (d_1 d_3/d_2^2)$.

For $\delta\phi' \ll 1$, we can solve equation (46) for the emission radius and obtain

$$r = \frac{r_{\rm LC}}{\nu_1}\delta\phi' - \frac{\nu_2 r_{\rm LC}}{\nu_1^3}\delta\phi'^2 + O(\delta\phi')^3. \tag{47}$$

5. DISCUSSION

There are many processes, such as aberration, retardation, and polar cap currents, that can collectively introduce a phase shift in the pulse components. The magnitudes of shifts due to each one of these processes can be estimated as on the order of r_n (see Gangadhara 2005, hereafter G05). In the radio emission regions, the relativistic phase shift $\delta\phi'_{\rm rps}$, on the order of r_n, is found to be less than unity. The polar cap current phase shift is found to be on the order of 3/2 near $\phi' \sim 0$ and less than 3/2 at large $|\phi'|$. The net phase shift $\delta\phi'$ due to aberration, retardation, and polar cap currents is on the order of unity in the regions close to $\phi' \sim 0$ and lies in the range 1–2 at large $|\phi'|$.

In the limit of the small-angle approximation ($\theta' \sim \zeta$), i.e., in the emission region close to the magnetic axis $\hat{\boldsymbol{m}}_t$ and for $r_n \ll 1$, it can be shown that our expression for the relativistic phase shift (eq. [34]) reduces to $r \approx (r_{\rm LC}/2)\delta\phi'_{\rm DRH}$ (eq. [7] in DRH04), where $\delta\phi'_{\rm DRH}$ is the relativistic phase shift. We can estimate $\delta\phi'_{\rm diff} = \delta\phi'_{\rm rps} - \delta\phi'_{\rm DRH}$, i.e., the difference in the phase shifts predicted by the two formulae. If $\delta\phi'_{\rm diff} = r_n^{\xi_{\rm diff}}$, then we have

$$\xi_{\rm diff} = \frac{\ln\left(\left|\delta\phi'_{\rm diff}\right|\right)}{\ln(r_n)}. \tag{48}$$

In Figure 12 we have plotted $\xi_{\rm diff}$ as a function of ϕ'. It shows that $\xi_{\rm diff}$ is $\sim$3/2 near $\phi' \sim 0$ and $\sim$1 at large $|\phi'|$, except in spiky regions.

Due to the rotational distortions such as the magnetic field sweepback of the vacuum dipole magnetic field lines, the relativistic phase shift is likely to be reduced. The magnetic field sweepback was first considered in detail by Shitov (1983). Recently, Dyks & Harding (2004) investigated the rotational distortions of a pulsar magnetic field by assuming the approximation of a vacuum magnetosphere. We used their expressions (eqs. [12] and [13] in Dyks & Harding 2004) to estimate the magnetic field sweepback:

$$\delta\phi'_{\rm mfsb} = \frac{\Delta\phi_{l-t}}{2} \approx \frac{2}{3}\sin\alpha\left[3\frac{xz}{r^2}\cos\alpha + \left(3\frac{x^2}{r^2} - 1\right)\sin\alpha\right]^{-1} r_n^3. \tag{49}$$

Using $x = r\sin\theta'\cos\phi'$ and $z = r\cos\theta'$, we computed $\delta\phi'_{\rm mfsb}$ for $\phi' = 50^\circ$, $\beta = 0^\circ$, and $\alpha = 10^\circ$ and 90°. It is found to be smaller than the aberration, retardation, and polar cap current phase shifts for $r_n < 0.2$ (G05). On the order of r_n, it is >3 in the case of $\alpha = 10^\circ$, while in the case of $\alpha = 90^\circ$ it lies in the range 2–3.

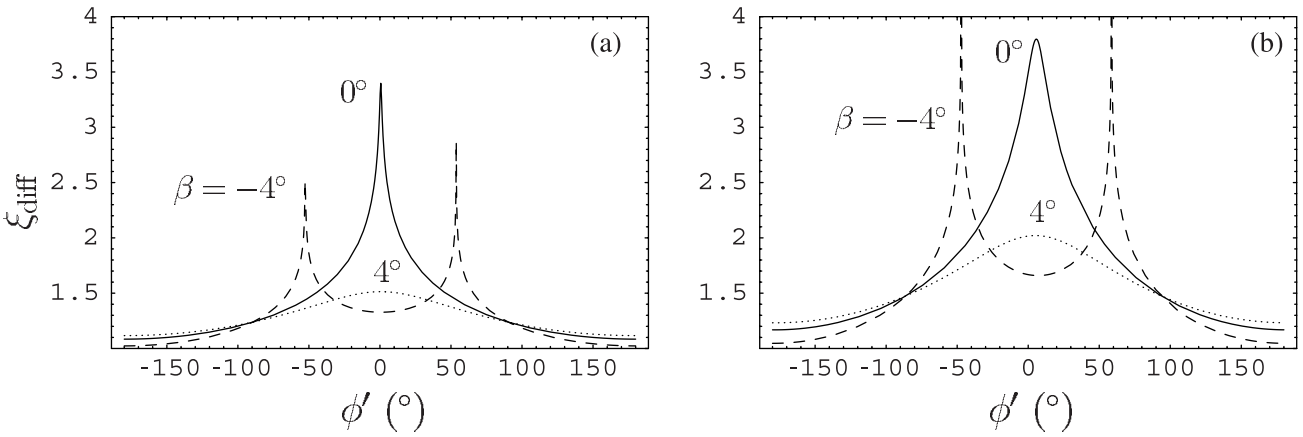

FIG. 12.—Index $\xi_{\rm diff}$ vs. phase ϕ' for (*a*) $\alpha = 10^\circ$ and $r_n = 0.01$ and (*b*) $\alpha = 10^\circ$ and $r_n = 0.1$.

In addition to the various processes that we have considered, the corotation of Goldreich-Julian charge density ($\eta_{\rm GJ}$) can also produce the phase shift. The corotating charges induce the magnetic field $\boldsymbol{B}_{\rm rot}$ given by

$$\nabla \times \boldsymbol{B}_{\rm rot} = \frac{4\pi}{c}\eta_{\rm GJ}\boldsymbol{\Omega} \times \boldsymbol{r} = \frac{4\pi}{c}\eta_{\rm GJ}\Omega r \sin\theta' \hat{\boldsymbol{\epsilon}}. \qquad (50)$$

Since both $\Omega r/c$ and $r\eta_{\rm GJ}/B_0$ are first order in r_n, $B_{\rm rot}/B_0$ becomes second order in r_n; therefore, we neglect the phase shift due to $\boldsymbol{B}_{\rm rot}$.

We may summarize that among the various phase shifts considered, the relativistic phase shift due to aberration-retardation is the dominant one. In the limit of the small-angle ($\beta \sim 0$) and low-altitude ($r_n \ll 1$) approximation, our expression for relativistic phase shift (eq. [34]) reduces to equation (7) given in DRH04. So, in the case of pulsars with small β and narrow profiles, one can use the expression (eq. [7]) given in DRH04 to estimate the emission heights, while for the pulsars with wide profiles or large β one has to use the revised phase shift given by our equation (45). The neglected effects such as the magnetic field lines' sweepback due to the reaction force exerted by the magnetic dipole radiation and the toroidal current due to the corotation of magnetosphere are of higher order than the proposed refinement.

For classical (normal) pulsars considered in GG01 and GG03, the revised emission heights are given in G05. The refinement (Δ) increases from the inner cone to outer cones for any given pulsar considered in Table 1 of G05. It is least (<1%) in the case of PSR 1237+25, but greater than 2% for all other pulsars, and maximum (13%) in PSR B2111+46. In some millisecond pulsars, the refinement can be quite significant. For example, in PSR J0437−4715 it is about 20%–60% (see Table 2 in G05).

6. CONCLUSION

We have derived a relation for the aberration phase shift that is valid for the full range of pulse phases. Although in the small-angle approximation we can show that the aberration phase shift becomes independent of parameters α and β, it does depend on α and β in the case of emissions from large rotation phases or altitudes. We have given a revised relation for the phase shift by taking into account aberration, retardation, and polar cap current. We find among the various phase shifts considered that the relativistic phase shift due to aberration-retardation is dominant.

I thank R. M. C. Thomas and Y. Gupta for discussions, J. Murthy for comments, and the anonymous referee for useful comments.

REFERENCES

Blaskiewicz, M., Cordes, J. M., & Wasserman, I. 1991, ApJ, 370, 643
Cordes, J. M. 1978, ApJ, 222, 1006
Dyks, J., & Harding, A. K. 2004, ApJ, 614, 869
Dyks, J., Rudak, B., & Harding, A. K. 2004, ApJ, 607, 939 (DRH04)
Gangadhara, R. T. 2004, ApJ, 609, 335 (G04)
———. 2005, preprint (astro-ph/0411161, ver. 2) (G05)
Gangadhara, R. T., & Gupta, Y. 2001, ApJ, 555, 31 (GG01)
Gil, J. A., & Kijak, J. 1993, A&A, 273, 563
Goldreich, P., & Julian, W. H. 1969, ApJ, 157, 869
Gupta, Y., & Gangadhara, R. T. 2003, ApJ, 584, 418 (GG03)
Hibschman, J. A., & Arons, J. 2001, ApJ, 546, 382
Kijak, J., & Gil, J. 2003, A&A, 397, 969
Lyne, A. G., & Manchester, R. N. 1988, MNRAS, 234, 477
Machabeli, G. Z., & Rogava, A. D. 1994, Phys. Rev. A, 50, 98
Phillips, J. A. 1992, ApJ, 385, 282
Radhakrishnan, V., & Cooke, D. J. 1969, Astrophys. Lett., 3, 225
Rankin, J. M. 1983a, ApJ, 274, 333
———. 1983b, ApJ, 274, 359
———. 1990, ApJ, 352, 247
———. 1993, ApJS, 85, 145
Ruderman, M. A., & Sutherland, P. G. 1975, ApJ, 196, 51
Shitov, Y. P. 1983, Soviet Astron., 27, 314
Sturrock, P. A. 1971, ApJ, 164, 529